Journal of Materials Chemistry C

Accepted Manuscript

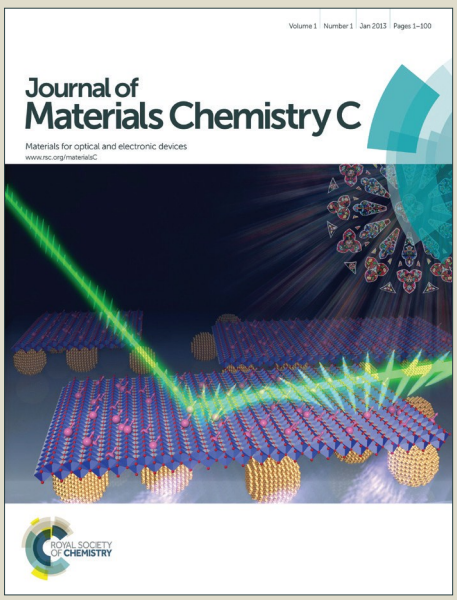

ROYAL SOCIETY OF CHEMISTRY

www.rsc.org/materialsC

Study of Ce^{3+} to Mn^{2+} energy transfer in highly transmission glasses by time-resolved spectroscopy

Susana Gómez-Salces[a,*], Jose Antonio Barreda-Argüeso[a], Rafael Valiente[b], and Fernando Rodríguez[a]
[a] *MALTA-CONSOLIDER-Team, DCITIMAC, Facultad de Ciencias, Universidad de Cantabria, 39005 Santander, Spain*
[b] *MALTA-CONSOLIDER-Team, Dpto. Física Aplicada, Facultad de Ciencias, Universidad de Cantabria, IDIVAL, 39005 Santander, Spain*

* Author for correspondence. E-mail: susana.gomez@unican.es

ABSTRACT

This work investigates the energy transfer from Ce^{3+} to Mn^{2+} in highly transmission glass (HTG) doped with CeO_2 and MnO through time-resolved spectroscopy to transform the solar spectrum into a more efficient red-enhanced spectrum for traditional Si-based solar cells. We show that both Mn^{3+} and Mn^{2+} and Ce^{3+} and Ce^{4+} centres are formed in HTG through their absorption and emission/excitation spectra. Interestingly, Ce^{3+} excitation at 320 nm yields both Ce^{3+} (400 nm) and Mn^{2+} (530 nm) emissions for doping concentrations of 0.1–1% Ce^{3+} and 0.1% Mn^{2+}. The energy transfer process in HTG is noteworthy since it enhances the capability for blue-to-red light transformation, what is important for concentrator in photovoltaic applications. This work analyses the non-radiative vs. radiative $Ce^{3+} \rightarrow Mn^{2+}$ energy transfer process in this optically enriched HTG. In the explored doping range we show that energy transfer is purely radiative.

Keywords: glasses; Ce^{3+}; Mn^{2+}; Mn^{3+}, photoluminescence; energy transfer; time-resolved spectroscopy, solar concentrators.

INTRODUCTION

Energy transfer (ET) among impurity ions in solids is the key for a considerable amount of studies related to the efficient use of energy. ET is important for applications in many fields such as communication devices,[1-4] phosphors,[5-6] solid state lasers[7-9] and in photovoltaic energy conversion. There is an increasing interest to investigate optically activated high transmission glasses (HTG) due to their capability as protector shields and solar spectrum transformers and concentrators for photovoltaic applications in Si solar cells.[10-14] By doping with adequately selected optically active centres, the HTG can transform the incoming photovoltaic-inefficient UV and IR solar radiation into visible (VIS) light, via downconversion (one UV photon $\rightarrow$ two VIS photon), upconversion (two IR photon $\rightarrow$ one VIS photon) or by large Stokes-shifted photoluminescence (PL) processes.[11-17] Depending on whether the selected dopants introduced in HTG are capable to efficiently absorb UV or IR radiation into photovoltaic useful VIS light, those enriched HTG can significantly improve the efficiency of the solar cells.

The spectroscopic properties of Ce^{3+} ions in different glasses are well known.[18-20] Ce^{3+} has a $4f^1$ ground state configuration, and shows very intense and efficient broadband luminescence upon excitation in the parity-allowed electric-dipole $4f \rightarrow 5d$ transition.[21] Because of their favourable spectroscopic properties and the ability to incorporate Ce^{3+} into different host materials, cerium activated materials, particularly, in glasses, have received considerable attention.[18-24]

The incorporation of MnO in fussed glasses, two valence states, Mn^{2+} and Mn^{3+}, are formed, the Mn^{2+}/Mn^{3+} ratio decreasing with the glass basicity.[24-25] Two structured Mn^{2+} ($3d^5$ electronic configuration) absorption bands results in 354 and 416 nm had been identified in sodium silicate glass.[26] Excitation into these bands gave rise to visible emission (520 nm) associated with the spin-forbidden *d–d* transition $^4T_1 \rightarrow {}^6A_1$ of Mn^{2+}.[27,28] On the other hand, Mn^{3+} ($3d^4$) did not show any photoluminescence and had an intense absorption band around 500 nm in binary silicate glasses strongly overlapping with the Mn^{2+} emission.[26] The intense Mn^{3+} broadband absorption at 500 nm corresponded to the parent octahedral $^5E \rightarrow {}^5T_2$ transition, whose levels were usually split by the low-symmetry crystal field acting at Mn^{3+} site as a consequence of either the low symmetry host site or the Jahn-Teller effect.[29] We co-dope our glass with CeO_2 to explore if Ce acts as reductor to favour Mn^{2+} formation over Mn^{3+}, or by contrast as an oxidant, favouring Mn^{3+} formation over Mn^{2+} through the two-way redox reaction: $Ce^{3+} + Mn^{3+} \leftrightarrow Ce^{4+} + Mn^{2+}$.[26]

In this work, we investigate the radiative vs. non-radiative nature of the Ce^{3+} to Mn^{2+} ET in CeO_2-MnO co-doped HTG through time-resolved spectroscopy. This doping intends to enhance the HTG capability for blue-to-red light transformation regarding photovoltaic applications. It must be noted that the interpretation of ET in glasses may be complicated by inhomogeneous band broadening. There are studies that showed the emission of Ce^{3+} in Ce^{3+}/Mn^{2+} co-doped phosphate glasses, decreased with increasing Mn^{2+} concentration.[28] The observation of Mn^{2+} emission at 594 nm upon excitation into the $4f \rightarrow 5d$ transition of Ce^{3+} at 307 nm suggested that such Mn^{2+} PL could be due to ET from Ce^{3+} to Mn^{2+}. In this respect, $Ce^{3+} \rightarrow Mn^{2+}$ ET has been observed in Zn_2SiO_4 and $SrAl_2O_3$ as key mechanism to get white efficient PL phosphors.[30,31,32] However non-radiative ET, which is activated by the electric dipole-quadrupole mechanism,[33] involves a critical average distance between Ce^{3+} and Mn^{2+} of 8.3 Å. Therefore, activation of this mechanism requires relatively high doping concentrations (approx. 30 weight %; much greater than 1 weight %). This work investigates whether Mn^{2+} PL under excitation into Ce^{3+} band at 320 nm in co-doped HTG, is induced by non-radiative ET from Ce^{3+} to Mn^{2+}, or it rises by direct excitation into Mn^{2+} crystal-field excited states from Ce^{3+} luminescence (radiative ET).

EXPERIMENTAL

High transmitting glass from GUARDIAN Sunguard Company was used. Recycled samples were ground glass as a host material and were mixed with different amounts of CeO_2 and MnO (Aldrich 97%). The mixture was deposited on alumina moulds with a subsequent thermal treatment at 1100ºC for 14 hours. It ensures a complete homogeneous incorporation of dopants into the host glass and prevent bubble formation. After thermal treatment, the glasses were annealed at 650 ºC to avoid crystallization by controlled cooling to ensure fully formation of amorphous glass. The samples were polished for spectroscopic studies. The host glass composition from x-ray fluorescence analysis is: SiO_2 (69.1 %wt), CaO (12.2 %wt), Na_2O (14.7 %wt), Al_2O_3 (2.7 %wt) with some traces of MgO, Fe_2O_3, K_2O and SO_3 (all traces are below 0.1 %wt). The density and refractive index (520 nm) of HTG are ρ = 2.5 g/cm^3 and n = 1.52, respectively. X-ray fluorescence analysis gives: CeO_2 (0.93%), MnO (0.09%) concentrations for

CeMnHTG. These results indicate that, within the experimental uncertainty, the nominal and actual concentration are the same. Table 1 summarizes the synthesized HTG prepared in this work. It should be noted that in this study CeO_2 concentrations is kept bellow 1% in weight in order to avoid as much as possible the formation of oxygen trapped inside of glass occurring at higher concentration and reducing dramatically the optical quality of the glass.

The main advantage of working with recycled glass is the reduction of the melting temperature (1100ºC) with respect to raw materials (1500ºC). The glass viscosity at 1100ºC is appropriated to homogeneously dissolve dopants in the bulk material. In any case, the viscosity is high enough to keep the melt in the mould without any leak.

The optical absorption spectra were taken with a CARY 6000*i* in the 200–1800 nm range and a PERKIN ELMER Lambda 9 in the 200–3200 nm spectral range. The spectra represent the average over four different sample orientations in order to minimize polarization effects and perpendicular misorientation of samples. This method, allows us an instrumental correction of the absorbance jumps attained by changing the photodetector from photomultiplier to IR detector (InGaAs and PbS, respectively).[34,35] This procedure permits measuring transmittances of 91.0% with accuracy better than 0.1%.
For photoluminescence measurements, the excitation, emission and time-resolved luminescence spectra were obtained with a FLSP920 (Edinburgh Inst.) spectrometer. All spectra were recorded a room temperature and corrected for the wavelength system response. The x-ray fluorescence analysis was obtained by means of an ARL ADVANT'XP (Thermo Scientific).

RESULTS AND DISCUSSIONS

Figure 1 shows the UV-Vis optical absorption spectra of HTG doped with different CeO_2 and MnO concentrations of (Table 1). The spectrum of undoped HTG is also shown to emphasize the Ce^{3+} and Mn^{3+} contribution to the spectra. The absorption band, appearing as a shoulder at 3.85 eV (322 nm) in CeHTG and CeMnHTG, corresponds to parity-allowed electric-dipole transition $4f \rightarrow 5d$ of Ce^{3+}.[27] A weak absorption band around 2.50 eV (500 nm) in MnHTG and CeMnHTG is also observed (inset of Figure 1). It corresponds to the $^5E \rightarrow {}^5T_2$ intraconfigurational transition of Mn^{3+} ($3d^4$) according to assignments given elsewhere.[36,37] The strong asymmetry of the absorption band between 1.5 and 2.5 eV reveals several absorption components, which are probably associated to the splitting of the Mn^{3+} $3d(e_g+t_{2g})$ energy levels, due to the strong low-symmetry crystal-field distortion produced by either the Jahn-Teller (JT) effect in sixfold coordination, or a smaller coordination number, e.g. N=5.[29] It must be noted that the absorption background increases in the visible region in CeMnHTG with respect to MnHTG thus indicating an increase of the glass basicity and of the $[Mn^{3+}]/[Mn^{2+}]$ ratio; *i.e.* CeO_2 acts as an oxidant for MnO in the redox reaction attained in CeMnHTG at high temperature.
Figure 2 shows the luminescence spectra of HTG doped with CeO_2 (CeHTG), MnO (MnHTG) and CeO_2-MnO (CeMnHTG) with concentrations given in Table 1. The emission/excitation spectra of CeHTG and MnHTG are shown in Figures 2A and 2B, respectively, while and the emission/excitation spectra of the doubly doped CeMnHTG in Figure 2C. Excitation spectra Figure 2B allow us to resolve Mn^{2+} bands despite the low Mn^{2+} concentration, which are not observed in the UV-VIS spectra (Figure 1) due to weak intensity of the Mn^{2+} bands. For singly doped Ce^{3+}HTG, there is a strong emission at 3.10 eV (400 nm) under UV excitation at 3.87 eV (320nm) with a long tail decreasing in the 2 -2.5 eV range (500 – 600 nm). This emission is ascribed to the parity-allowed transition of the lowest component of the 5*d* state to $^2F_{5/2}$ and $^2F_{7/2}$ levels of Ce^{3+} ions.[21] The emission is associated with a strong excitation band at 3.7 eV (335 nm) corresponding to $4f \rightarrow 5d$ transition of Ce^{3+}. For Mn^{2+} singly doped HTG (Figure 2B), an intense emission band at 2.34 eV (530 nm) with a shoulder at 1.9 eV (650nm) is observed. The corresponding excitation spectra are also shown in Figure 2B. According to band assignment given elsewhere,[27,28] the band shape and transition energy of these bands at 2.77, 2.89, 2.96, 3.32, 3.50 and 3.71 eV can be unambiguously assigned to tetrahedrally coordinated Mn^{2+}. Within T_d symmetry these bands correspond to Mn^{2+} *d-d* transitions from the $^6A_1$(S) ground state to mainly $^4T_1$(G), $^4T_2$(G), $^4A_1{}^4E$(G), $^4T_2$(D), ^4E(D) and $^4T_1$(P) excited states, respectively.[38] The crystal-field parameters obtained by fitting the experimental transition energies to the calculated energies for d^5 electronic configuration are given together with the Tanabe-Sugano diagram in Figure 3. Due to the strong emission of Ce^{3+} in CeMnHTG (Figure 2C), the emission of Mn^{2+} (around 2.34 eV) is masked in this spectrum.[28] However, the superimposed weak emission intensity to the Ce^{3+} band emission in the 2–2.5 eV range can probably

include the contribution from Mn^{2+} emission. In fact, the excitation spectrum associated with the emission at 2.34 eV (530 nm) shows clearly Mn^{2+} excitation peaks. Indeed, the excitation spectrum, apart from the broad intense band at 3.7 eV (335 nm) corresponding to $4f \rightarrow 5d$ transition of Ce^{3+}, which is the major luminescence feature, some additional less-intense excitation bands are observed between 2.75–3.00 eV (450–410 nm), which coincides with the Mn^{2+} excitation peaks of Figure 2B. Interestingly, there is a strong overlap between Ce^{3+} emission and Mn^{2+} excitation (Figure 2C) that according to Förster theory fulfills ideal resonance conditions for an efficient ET between Ce^{3+} (donor) and Mn^{2+} (acceptor).[39,40] The strong Ce^{3+} band at 3.7eV in the excitation spectrum which is associated with the green emission at 2.34 eV (530 nm), clearly indicates that ET from Ce^{3+} to Mn^{2+} is likely. In order to elucidate the radiative vs. non-radiative nature of the Ce^{3+} to Mn^{2+} ET, we have performed time-resolved emission and excitation spectroscopy study.

Time-resolved spectroscopy allows us to unveil the presence of different Mn^{2+} centers in HTG as well as unambiguously demonstrates the existence of $Ce^{3+} \rightarrow Mn^{2+}$ ET. Figure 4 shows the luminescence intensity decay curves $I(t)$ corresponding to the green (2.34 eV) and red (1.91 eV) emissions of Mn^{2+}. Two different average exponential decays for $I(t)$ are observed with associates lifetimes of 9.1 and 13.4 ms for green and red emissions, respectively. It means that not only inhomogeneously distributed fourfold and/or fivefold coordinated centres are observed, but also other probably six-fold coordinated Mn^{2+} centres, which are subjected to higher crystal-field strengths than T_d or C_{4v} centres. Hence, red and green PL emissions are attained at the same time. Figures 2 and 4 clearly demonstrate that the short lived green emission corresponds to the broad emission centred at 2.34 eV (530 nm), the excitation of which is characteristic of T_d (or nearly T_d) centres. Analogously, the long lived red emission corresponds to a weaker broad emission band peaking at 1.91 eV (650 nm), whose excitation spectrum, rather than T_d, is probably related to a nearly octahedral coordination. This assignment is based on the shift of the first transition energy towards lower energies, unveiling a higher crystal-field splitting parameter (Δ > 0.7 eV) than that measured for T_d Mn^{2+} (Δ = 0.42 eV), as expected for a nearly octahedral coordination.
Figure 5 shows the time-resolved emission (A) and excitation (B) spectra of MnHTG and CeMnHTG. Both spectra are taken under pulsed excitation with delay times longer than 200 μs to permit a complete deexcitation of Ce^{3+} (τ = 1–5 ns) before detection.[23,28,39] With this procedure we detect emissions whose lifetimes are longer than about 200 μs as for example Mn^{2+} (τ = 10 ms) or intrinsic defects in the glass matrix.[41,42] Other shorter-lived emissions like Ce^{3+} do not contribute to luminescence spectra. The time-resolved emission spectra of CeMnHTG under selective excitation into the Ce^{3+} band (3.87 eV — 320 nm) consists mainly of Mn^{2+} green emission at 2.34 eV (530 nm) whereas, the intense Ce^{3+} emission at 3.10 eV (400 nm) is completely absent. It must be noted that excitation at 3.87 eV is unable to excite Mn^{2+} in MnHTG (Figures 3 and 5B), but induces Mn^{2+} photoluminescence in CeMnHTG (Figure 5A), thus evidencing $Ce^{3+} \rightarrow Mn^{2+}$ ET in this system. A residual emission band at 3.00 eV (413 nm), which is also observed in the undoped HTG (Figure 5A), is probably associated with defects of oxygen deficiencies in the glasses.[41,42]
The time-resolved excitation spectra of Figure 5B reveal a radiative ET from Ce^{3+} to Mn^{2+} while the non-radiative ET mechanism is completely ruled out in these HTG samples. In order to demonstrate it we must consider that excitation spectroscopy was accomplished using a pulsed Xe lamp by detecting green emission at 2.34 eV (530 nm) with delay and gate times of 200 μs and 40 ms, respectively. Under such detection conditions, the intense Ce^{3+} excitation band observed at 3.87 eV (320 nm) in the cw excitation spectra (Figure 2C), is notably reduced by an order of magnitude with respect to the Mn^{2+} excitation intensity in the time-resolved spectra. In fact, the excitation spectrum fully corresponds to T_d Mn^{2+} peaks (Figures 4 and 5B) in MnHTG, while the excitation of CeMnHTG shows an additional weak excitation broad band at 3.7 eV (335 nm) corresponding to Ce^{3+}. The difference between time-resolved excitation spectra CeMnHTG and MnHTG shown in Figure 5B confirms it. This result is noteworthy since it means that the intense Ce^{3+} band observed in the cw excitation spectrum detecting at 2.34 eV (Figure 2C) does not entirely correspond to Mn^{2+} emission but also to Ce^{3+} emission, particularly, in the low energy tail component of the 3.10 eV emission band. Therefore, the Ce^{3+} to Mn^{2+} excitation intensity ratio, $I_{3.7eV}(Ce^{3+}) / I_{2.9eV}(Mn^{2+})$, changes from 5 under cw excitation to 0.44 in time-resolved excitation. So the Ce^{3+} relative intensity decreases by a factor 11 using a delay time of 200 μs. Such an intensity reduction factor is consistent with a radiative ET mechanism.
Indeed, this reduction factor can be accounted for on the basis of Mn^{2+} emission induced directly by exciting Mn^{2+} centres with light coming from Ce^{3+} emission (direct radiative ET). Figure 6 shows Ce^{3+} emission band under excitation at 3.87 eV (320 nm) together with the Mn^{2+} excitation spectrum

obtained in MnHTG to illustrate the resonance conditions for Ce^{3+} to Mn^{2+} ET. From these spectra the fraction of Ce^{3+} emitted photons, which are absorbed by Mn^{2+} in a 1 mm thickness CeMnHTG sample, is 2×10^{-4} I_0 with I_0 being the Ce^{3+} emission intensity at the band maximum (3.10 eV). Therefore, the number of Mn^{2+} emitted photons by direct absorption of the Ce^{3+} luminescence (radiative ET) is 2×10^{-4} I_0. However, it must be noted that the Ce^{3+} excitation intensity of Figure 2C corresponds only to a small fraction of the total Ce^{3+} emission intensity: the excitation intensity is obtained by light detection at 530 nm using spectral slits of 2 nm. It means the excitation intensity at the band maximum at 3.7 eV (335 nm) corresponds to a fraction of $1/(40\times12.5) = 2\times10^{-3}$ of the total Ce^{3+} emission intensity. Therefore the ratio of Ce^{3+}/Mn^{2+} emitted photons (referred to the Mn^{2+} peak intensity at 2.9 eV) by radiative ET is: 2×10^{-3} I_0 / 2×10^{-4} I_0 = 10, which is in fair agreement with the reduction factor of 11 obtained by comparing the cw and time-resolved excitation spectra of CeMnHTG of Figures 2C and 5B.

This result points out that non-radiative Ce^{3+} to Mn^{2+} ET in CeMnHTG below the saturation concentration of dopants (1% for Ce and 0.1% for Mn) is unlikely. In this concentration range, ET is mainly achieved through a radiative mechanism, the non-radiative ET being inefficient. Actually, the non-radiative ET would be efficient and dominant ET mechanism for Ce and Mn concentrations of about 30%. In fact, the non-radiative ET probability is expected to be very small for detection since the average Ce – Mn distance in the more doped HTG (1%Ce – 1%Mn) is about 25 Å, which is about 3 times longer than the critical distance for non-radiative ET: R_0 = 8.3 Å.[33] In conclusion, there exist a radiative ET from Ce^{3+} to Mn^{2+} in doubly Ce, Mn-doped HTG allowing a partial transformation of the Ce^{3+} UV emission into visible (530 nm) emission from Mn^{2+}.

CONCLUSIONS

By means of optical absorption and time-resolved photoluminescence, we have identified two valence states of manganese: Mn^{2+} and Mn^{3+} in HTG doped with CeO_2 and MnO. We demonstrate that Ce^{3+} and Mn^{2+} fulfill ideal conditions for energy transfer since the corresponding emission and excitation spectra largely overlap. We show that there exist and Ce^{3+} to Mn^{2+} ET in CeMnHTG, although for the explored doping concentrations (0.1–1 weight %) the ET mechanism is purely radiative. A salient result emerging from this work is that an efficient solar transformer HTG based on the Ce and Mn should be achieved by incorporating local concentrations of Ce and Mn of about too high 30% as a way of activating the non-radiative ET mechanism, but keeping the transmission performances of the glass in the VIS-NIR. An efficient method to get such high dopant concentration locally can be achieved by embedding optically active Ce– and Mn–doped oxide nanoparticles with concentrations of about 30% during the glass fabrication process. This way will provide more efficient non-radiative HTG Ce-Mn ET processes, thus enhancing the solar spectrum transformation capabilities. Investigations with this target are currently in progress.

ACKNOWLEDGEMENTS

This work has been done within a collaborative Research in photovoltaic glasses with the R & D Centre, Saint-Gobain, Avilés (Spain). We thank financial support from the Spanish Ministerio of Economía y Competitividad (Project No. IPT-2011-1868-920000).

REFERENCE

1 F. Lahoz, E. Daran, G. Lifante, T. Balaji and A. Muñoz-Yague, *Appl. Phys. Lett*., 1999, **74**, 1060.
2 P.S. Golding, S.D. Jackson, T. King and M. Pollnau, *Phys. Rev. B*, 2000, **62**, 856.
3 C. Strohhofer, P.G. Kik and A. Polman, J. *Appl. Phys*., 2000, **88**, 4486.
4 S.H. Park, D.C. Lee, J. Heo and D.W. Shin, *J. Appl. Phys*., 2002, **91**, 9072.
5 D. Jia, R.S. Meltzer, W.M. Yen, W. Jia and X. Wang, *Appl. Phys. Letter* ,2002, **80**, 1535.
6 E.J. Bosze, G.A. Hirata, L.E. Shea-ohwer and J. McKittrick, *J. Lumin*., 2003, **104**, 47.
7 A. Braud, S. Girard, J. L. Doualan, M. Thuau, R. Moncorgé and A. M. Tkachuk., *Phys.Rev. B*, 2000, **61**, 5280.
8 J.T. Vega-Duran, L.A. Diaz-Torres, M.A. Meneses-Nava, J.L. Maldonado-Rivera and O. Barbosa-Garcia, *J. Phys. D: Appl. Phys*., 2001, **34**, 3203.

9 G.V. Vázquez, R. Valiente, S. Gómez-Salces, E. Flores-Romero, J. Rickards and R. Trejo-Luna, *Opt. Laser Technol*., 2016, **79**, 132.
10 S. Gómez, I. Urra, R. Valiente and F. Rodríguez, *Sol. Energy Mater. Sol. Cells*, 2011, **95**, 2018.
11 B.S. Richards, *Sol. Energy Mater. Sol. Cells*, 2006, **90**, 1189.
12 C. Strümpel, M. McCann, G. Beaucarne, V. Arkhipov, A. Slaoui, V. Švrček, C. del Cañizo and I. Tobias, *Sol. Energy Mater. Sol. Cells*, 2007, **91**, 238.
13 C. R. Ronda, *J. Alloys Compd*., 1995, **225**, 534.
14 M. Green, Springer, Berlin, 2003.
15 M. A. García, E. Borsella, S. E. Paje, J. Llopis, M. A. Villegas and R. Polloni, *J. Lumin*., 2001, **93**, 253.
16 M. Nogami, T. Yamazaki and Y. Abe," *J. Lumin*., 1998, **78**, 63.
17 Y. K. Sharma, S. S. L. Surana, R. K. Singh and Indian *J. Pure Appl. Phys*., 2008, **46**, 239.
18 G. C. Kim, S. I. Mho and H. L. Park, *J. Mater. Sci. Lett*., 1995, **14**, 805.
19 D. Curie, Luminescence in crystals, Methuen and Co Ltd, London, 1963.
20 J. S. Stroud, *J. Chem. Phys*., 1961, **35**, 844.
21 S. E. Paje, M. A. García, M. A. Villegas and J. Llopis, *Opt. Materials*, 2001, **17**, 459.
22 M. J. Weber, M. Bliss, R. A. Craig and D. S. Sunberg, *Radiat. Eff. Defects Solids*, 1995, **134**, 23.
23 J. Bei, G. Qian, X. Liang, S. Yuan, Y. Yang and G. Chen*, Mater. Res. Bull*., 2007, **42**, 1195.
24 S.P. Singh, Aman and A. Tarafder, *Bull. Mater. Sci*., 2004, **27**, 281.
25 W. Thiemsorn, K. Keowkamnerd, S. Phanichphant, P. Suwannathada and H. Hessenkemper, *Glass Phys. and Chem*., 2008, **34**, 19.
26 J. M. Fernández, "*El vidrio*" 2º edition CSIC, Madrid, 1991.
27 C. F. Song, M. K. Lü, P. Yang, F. Gu, D. Xu and D. R. Yuan, *J. Sol-Gel Sci. Technol*, 2003, **28**, 193.
28 P. I. Paulose, G. Jose, V. Thomas, N. V. Unnikrishnan and M. K. R. Warrier, *J. Phys. Chem. Solids*, 2003, **64**, 841.
29 M-N. Sanz-Ortiz and F. Rodríguez, *J. Chem. Phys*., 2009, **131**, 124512.
30 R. Ye, H. Mab, C. Zhanga, Y. Gao, Y. Huaa, D. Denga, P. Liub and S. Xu, *J Alloys Compd*, 2013, **566**, 73.
31 X. Xu, Y. Wang, X. Yu, Y. Li and Y. Gong, *J. Am. Ceram. Soc.,* 2011, **94**, 160.
32 G. Li, D. Geng, M. Shang,C. Peng, Z. Chenga and J. Lin, J. Mater. Chem., 2011, **21**, 13334.
33 E. Nakazawa and S. Shionoya, *J. Chem. Phys.,* 1967, **47**, 3211.
34 S. Gómez, I. Urra, R. Valiente and F. Rodriguez, *J. Phys.: Condens. Matter*, 2010, **22**, 295505.
35 S. Gomez-Salces, PhD Thesis, University of Cantabria 2012.
36 N. Da, M. Peng, S. Krolikowski and L. Wondraczek, *Opt. Express*, 2010, **18**, 2549.
37 S. Kück, S. Hartung, S. Hurling and K. Petermann, G. Huber, *Phys. Rev. B*, 1998, **57**, 2203.
38 Y. Rodríguez-Lazcano, L. Nataf and F. Rodríguez, *Phys. Rev. B*, 2009, **80**, 085115.
39 Y. Yu, Z. Liu, Y. Sheng, H. Luan, J. Peng, Z. Jiang, H. Li, J. Li and L. Yang, *Opt. Express*, 2011, **19**, 19473.
40 Th. Förster, *Ann. Physik*, 1948, **437**, 55.
41 T. Hayakawa, A. Hiramitsu and M. Nogami, *Appl. Phys. Lett.*, 2003, **82**, 2975.
42 J. Zhou, G. Sun, H. Zhao, X. Pan, Z. Zhang, Y. Fu, Y. Mao and E. Xie, *J. Nanotechnol*., 2015, **6**, 313.

TABLE CAPTION

Table 1. Nominal concentration of CeO_2 and MnO (weight %) for different high-transmission glasses (HTG).

FIGURE CAPTIONS

Figure 1. Room-temperature optical absorption spectra of MnHTG (– – – –), CeHTG (-- ·--·), CeMnHTG (·····) and undoped HTG (——) in the 1.5–4.5 eV range. The inset shows the corresponding absorption of Mn^{3+} in the 1.5–3.0 eV range.

Figure 2. Emission (———) and excitation (– – – – and ·····) spectra under cw excitation of CeHTG (A), MnHTG (B) and CeMnHTG (C). Spectral resolution: $\Delta\lambda$ = 2 nm.

Figure 3. Excitation spectrum of Mn^{2+} of HTG doped with 0.1% MnO (red points) associated with the green emission at 530 nm. The spectrum can be simulated (blue line) as the sum of Gaussian shaped bands (dashed lines) within a T_d crystal-field splitting of states with transition energy at 2.77, 2.89, 2.96, 3.32, 3.50 and 3.71 eV. The crystal-field parameters derived from the Tanabe-Sugano diagram (d^5) are B = 0.081 eV; C = 0.42 eV; Δ = 0.42 eV. The experimental transition energies with associated bandwidths (red rectangles) and calculated energies are compared in the Tanabe-Sugano diagram shown above the spectrum.

Figure 4. Luminescence time-dependence, $I(t)$, corresponding to the green emission at 2.34 eV (530nm) and red emission at 1.91 eV (650nm) to Mn^{2+} of MnHTG samples. Lifetimes values correspond to fits of the experimental points to average exponential decay behaviour of $I(t)$. The fit includes instrumental response due to the pulsed Xe lamp and background correction.

Figure 5. Time-resolved excitation/emission spectra of MnHTG and CeMnHTG. A) Time-resolved emission of CeMnHTG (– · – · – ·) and undoped HTG (——) by excitation at 3.87 eV (320 nm). B) Time-resolved excitation spectra corresponding to the green emission at 2.34 eV (530nm) in CeMnHTG (——) and MnHTG (– – – –). The pointed spectrum (·····) correspond to subtraction of time-resolved excitation spectra CeMnHTG and MnHTG. Both excitation and emission spectra were accomplished using a pulsed Xe lamp using delay and times for detection of 200 µs and 40 ms, respectively.

Figure 6. Emission spectrum (——) of CeHTG by excitation at 3.87 eV (320nm) and excitation spectrum (– – – –) of MnHTG. The absorption coefficient scale for Mn^{2+} was obtained from optical absorption measurements in 1 mm-thickness MnHTG sample.

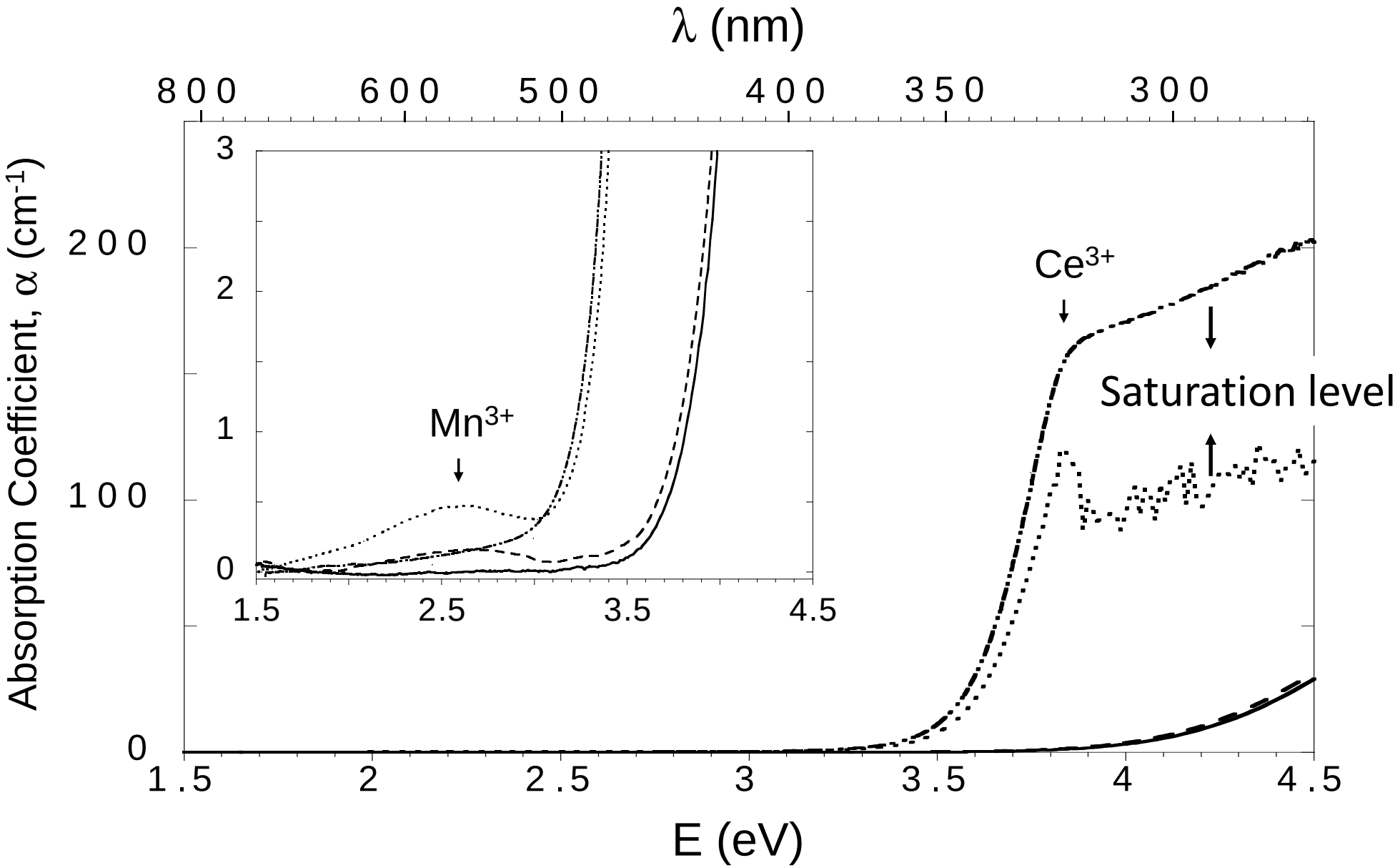

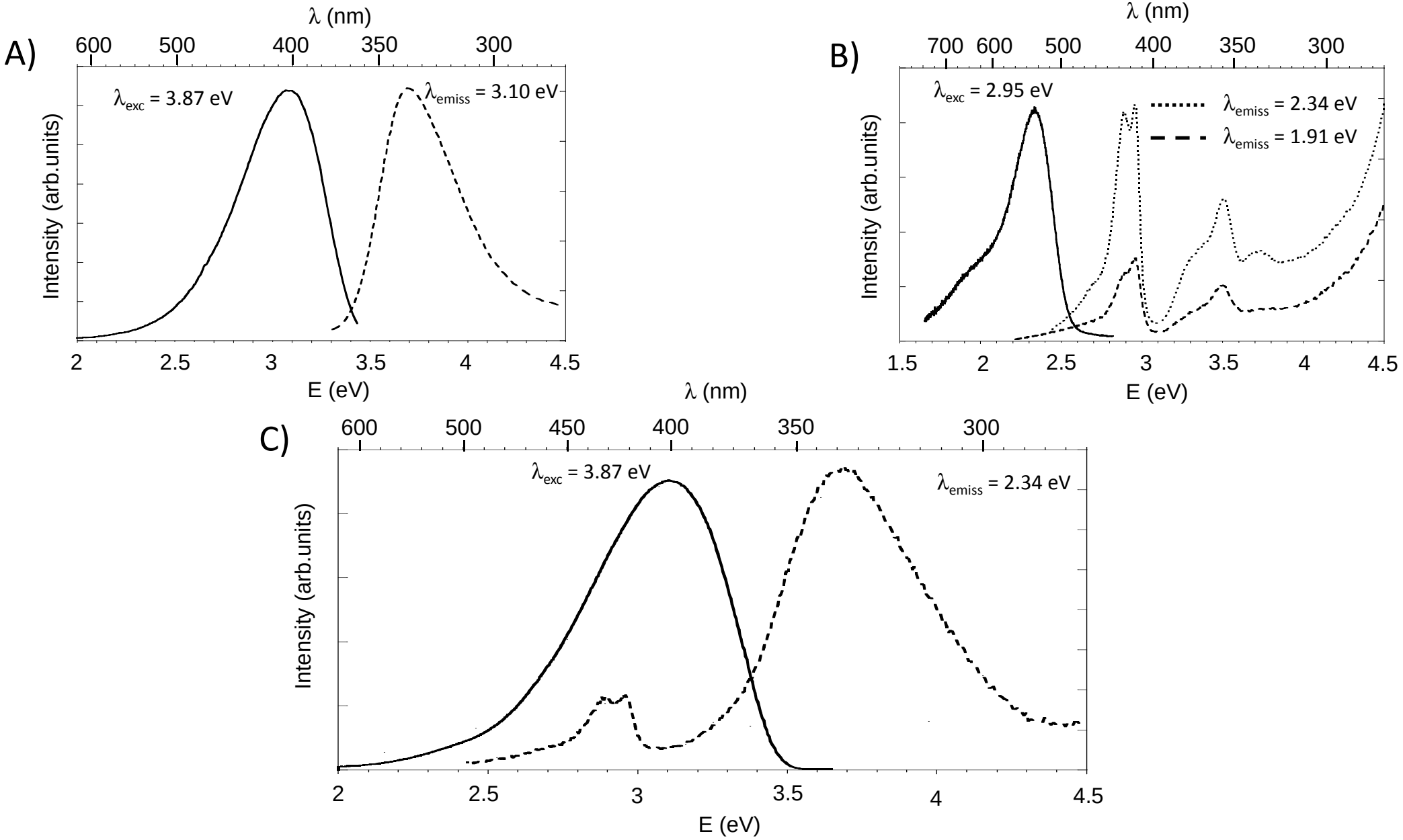

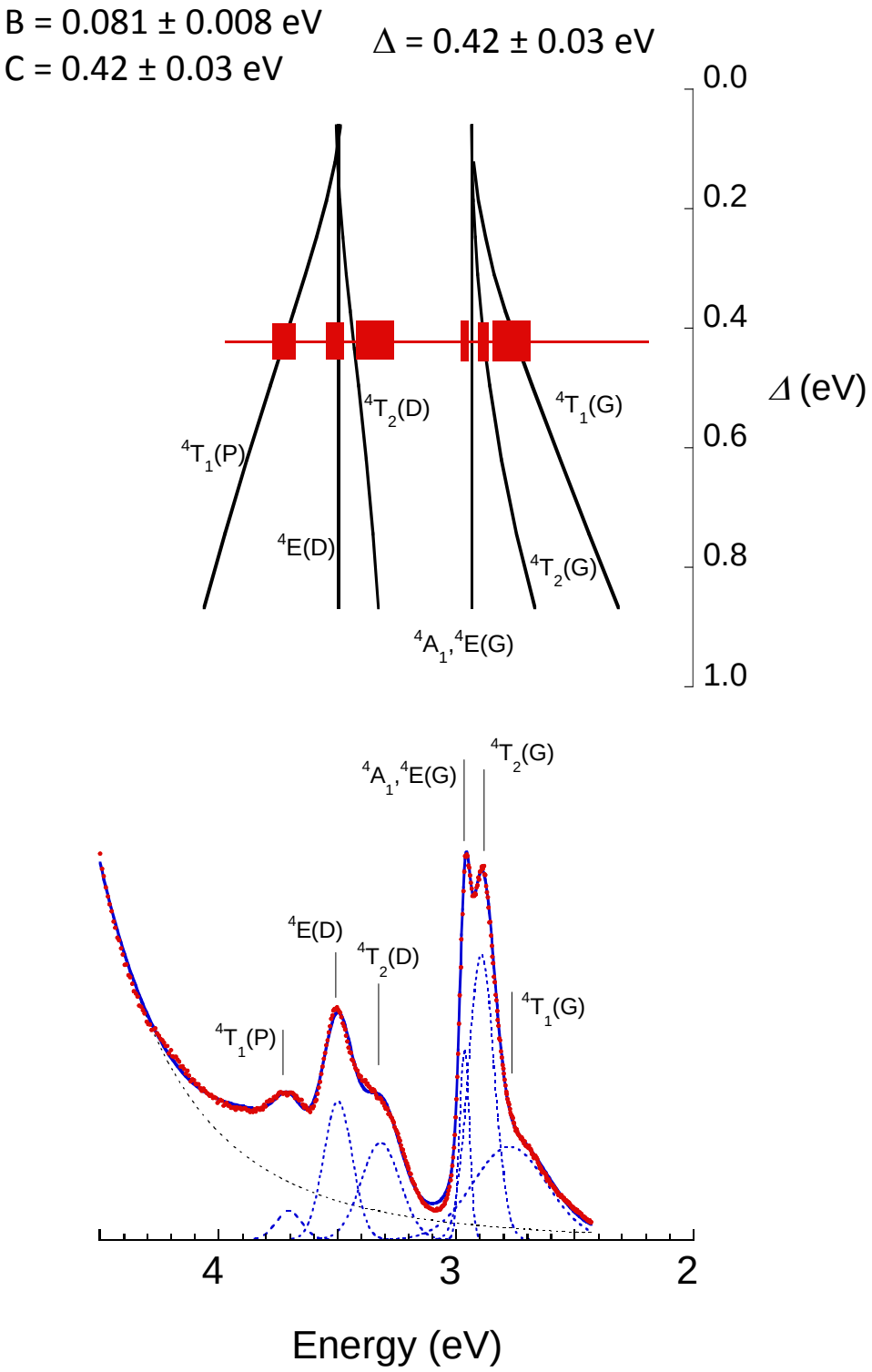

Figure 3.

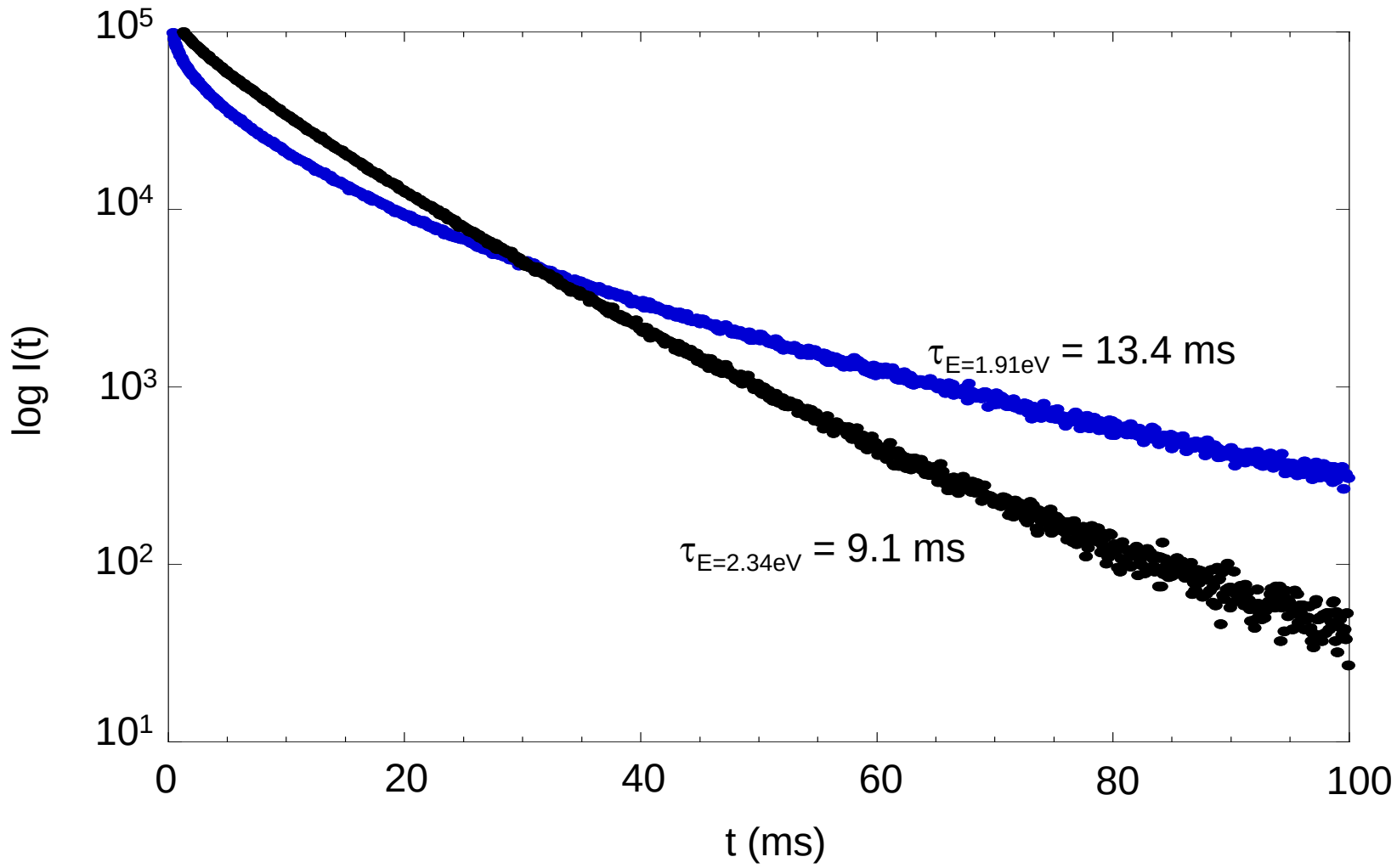

Figure 4.

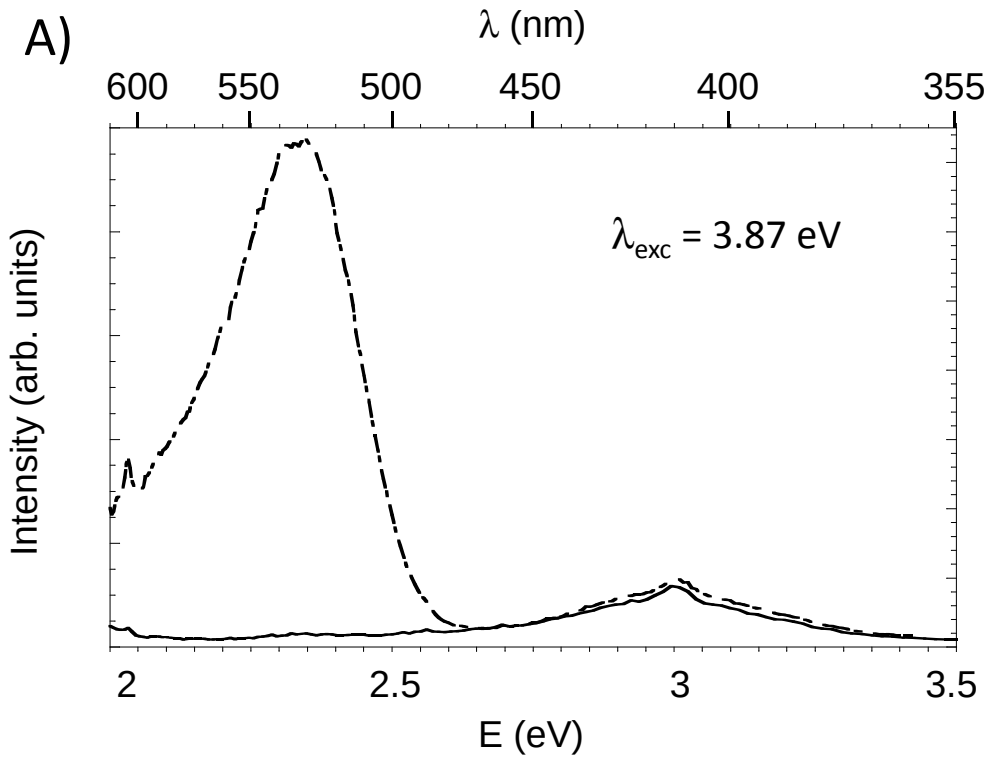

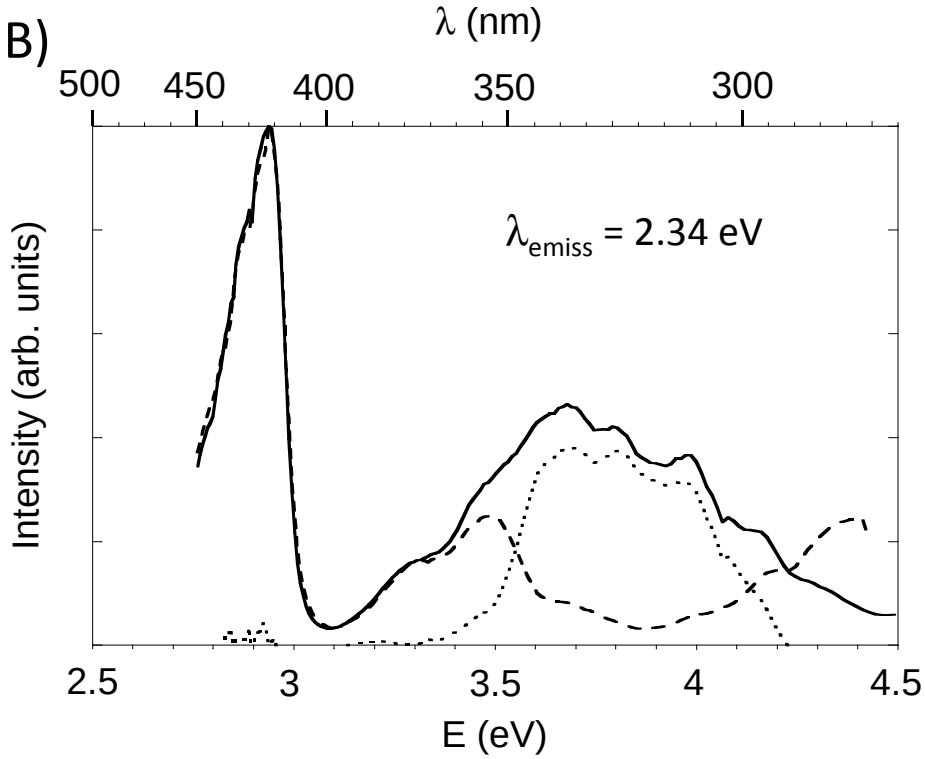

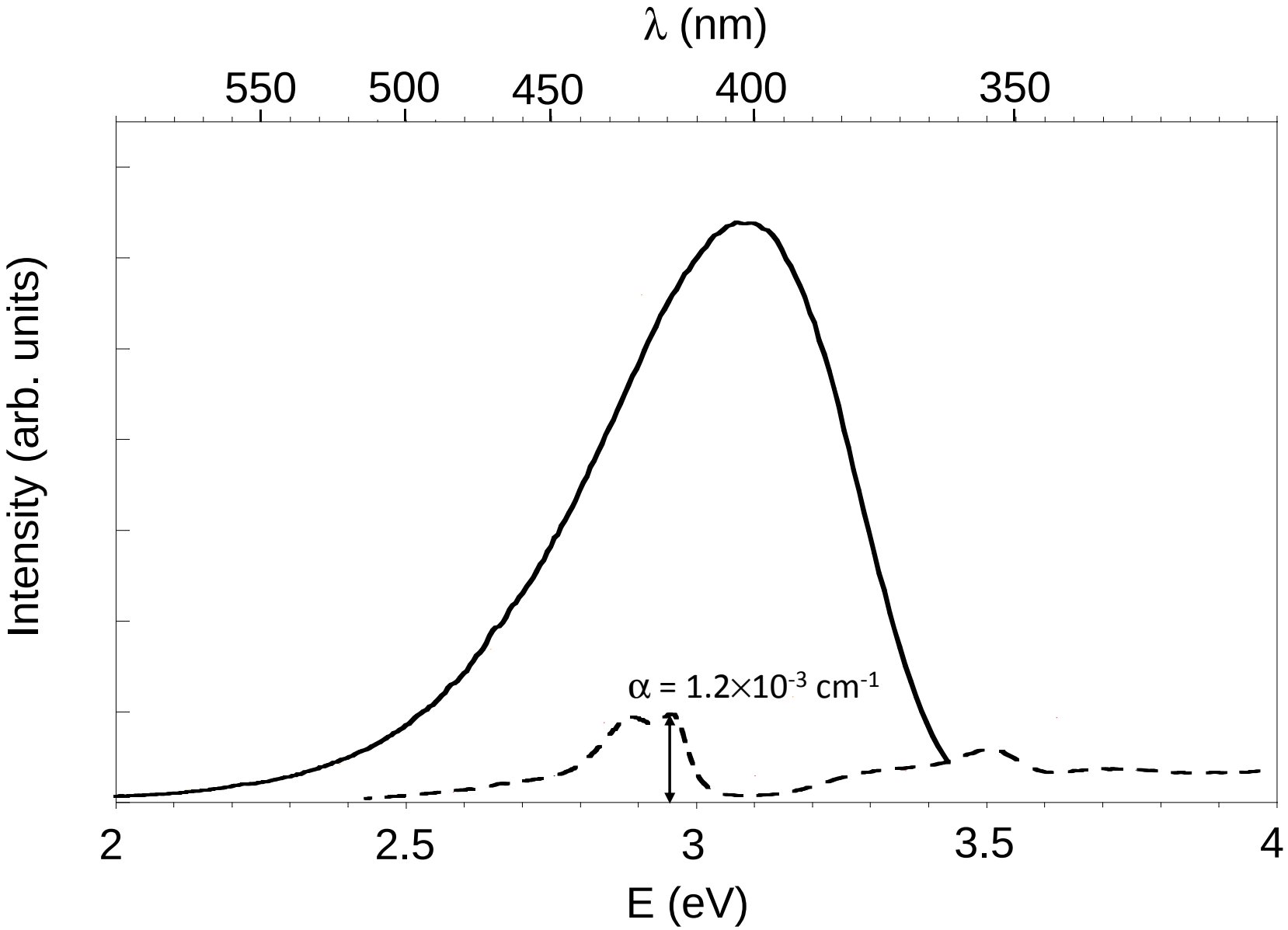

TABLES

Table1. Nominal concentration of CeO_2 and MnO (weight %) for different high-transmission glasses (HTG).

Sample code	MnHTG	CeHTG	CeMnHTG
CeO_2 (wt.%)	-	1.0	1.0
MnO (wt.%)	0.1	-	0.1